ARTICLE

TECHNOLOGY

Automated end-to-end blood testing at the point-of-care: Integration of robotic phlebotomy with downstream sample processing

M.L. Balter, J.M. Leipheimer, A.I. Chen, A. Shrirao, T.J. Maguire & M.L. Yarmush

Diagnostic blood testing is the most commonly performed clinical procedure in the world, and influences the majority of medical decisions made in hospital and laboratory settings. However, manual blood draw success rates are dependent on clinician skill and patient physiology, and results are generated almost exclusively in centralized labs from large-volume samples using labor-intensive analytical techniques. This paper presents a medical device that enables end-to-end blood testing by performing blood draws and providing diagnostic results in a fully automated fashion at the point-of-care. The system couples an image-guided venipuncture robot, developed to address the challenges of routine venous access, with a centrifuge-based blood analyzer to obtain quantitative measurements of hematology. We first demonstrate a white blood cell assay on the analyzer, using a blood mimicking fluid spiked with fluorescent microbeads, where the area of the packed bead layer is correlated with the bead concentration. Next we perform experiments to evaluate the pumping efficiency of the sample handling module. Finally, studies are conducted on the integrated device — from blood draw to analysis — using blood vessel phantoms to assess the accuracy and repeatability of the resulting white blood cell assay.

***Keywords*: Medical Robotics; Venous Access; Point-of-Care Blood Testing; Microscale Sample Processing; Centrifugal Microfluidics.**

1. INNOVATION

Despite recent progress in robotics, automation, and *in vitro* diagnostics, no end-to-end solution for complete point-of-care testing (POCT) exists today. With the advent of miniaturized robotic and microfluidic systems, the technology is in place to combine the breadth and accuracy of traditional laboratory testing with the speed and convenience of POCT. Our group is developing a platform device that enables end-to-end testing by performing blood draws and providing diagnostic results in a fully automated fashion. By reducing turnaround times, the device also has the capacity to expedite hospital work-flow, allowing practitioners to devote more time to treating patients.

2. INTRODUCTION

Diagnostic blood testing is the most common medical routine performed in the world, and in many ways, forms the cornerstone of modern medicine[1]. In the U.S., blood tests are performed 2 billion times each year and influence 80% of medical decisions made in hospital and primary care settings[2,3]. However, blood draw success rates depend heavily on practitioner skill and patient physiology, and diagnostic results are generated almost exclusively in centralized labs from large-volume blood samples using labor-intensive analytical techniques[4].

Traditionally, blood is first drawn manually by venipuncture, samples are transported to a centralized lab, and then the analysis is performed before results are finally returned to the medical staff to guide the intervention. Logistically, this is a complicated process, especially considering the sheer volume of tests performed on a regular basis. Unexpected delays and errors can arise due to difficulties in performing the venipuncture and from inefficiencies during the transport and subsequent analysis of the blood sample. Such delays have been shown to reduce specimen quality and increase turnaround times, potentially leading to erroneous test results[5–8]. Delays are particularly common in difficult patients, such as children, elderly, chronically-ill and obese populations, where small and fragile vessels or high levels of body fat may reduce the visibility of veins or make them more difficult to accurately puncture[9–11].

To reduce turnaround times and expedite the clinical decision making process, POCT has emerged as an alternative approach[12,13]. One of the potential benefits of POCT is that traditional laboratory venipuncture can be replaced by a finger-prick capillary draw, which requires much less skill to perform and removes a significantly smaller volume of blood. Commercially available devices have been developed for many assays. For example, handheld analyzers such as the iSTAT device[12,14] use disposable cartridges to assess basic chemistry, blood gases, and protein markers, primarily using capillary blood from the finger. Automated cell counters such as the Chempaq XBC[15] and HemoCue WBC[16] have also been introduced to perform cell counts from capillary blood. However, the main limitation with POCT analyzers is the reliance on capillary blood from finger-pricks. Specifically, the accuracy and standardization

Department of Biomedical Engineering, Rutgers University, Piscataway NJ 08854, USA. Correspondence should be addressed to M.L.B. (balterm53@gmail.com).

Received 22 January 2018; accepted 7 May 2018; published online 30 May 2018; doi:10.1142/S2339547818500048

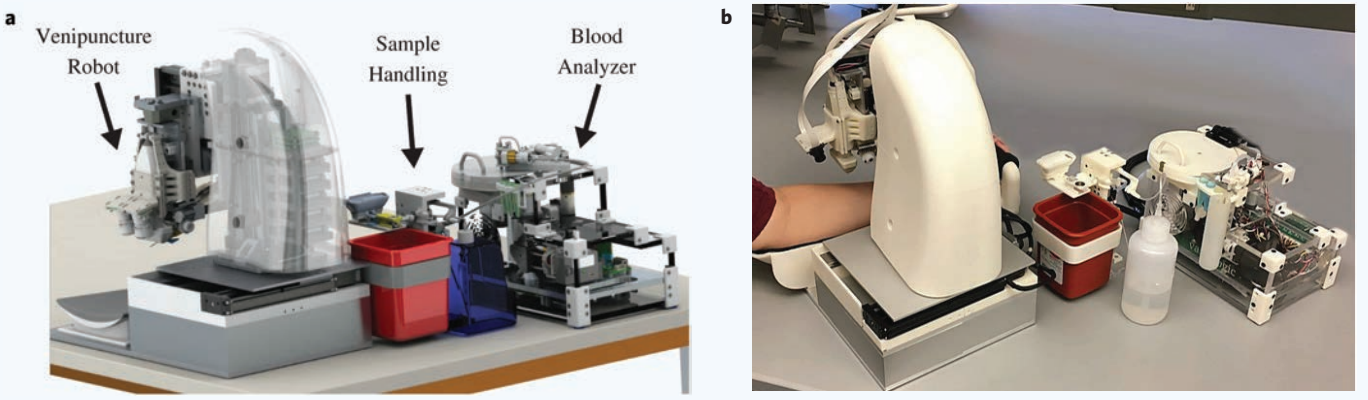

Figure 1 (**a**) Design concept and (**b**) implementation of the automated blood testing and analysis device.

of capillary-based measurements compared to venous samples is still a matter of debate[17,18]. Furthermore, POCT analyzers often require manual sample preparation and, on some tests, provide measurements with limited sensitivity and dynamic range compared to bench-top analyzers[19,20].

Additionally, the quest to achieve an end-to-end solution in blood testing has driven the adoption of robotic solutions across many diagnostic facilities[21,22]. Lab automation systems, including tube handling devices, pipetting instruments, and hematology analyzers, have been developed to improve efficiency and reduce human error within centralized facilities[23,24]. However, these systems are large, expensive, and decoupled from the blood sampling process, thus limiting their applicability in POCT settings.

Our group is developing a medical device that enables end-to-end blood testing by performing blood draws and providing diagnostic results in a fully automated fashion at the point-of-care. The system couples an image-guided venipuncture robot, developed to address the challenges of routine venous access, with a microcentrifugation and optical detection platform that performs the diagnostic analysis. The device, as seen in **Fig. 1**, comprises three distinct sub-systems: a robotic venipuncture device, sample handling module, and centrifuge-based blood analyzer. **Table 1** summarizes the key features of the integrated device.

The venipuncture robot uses Near-infrared (NIR) and Ultrasound (US) imaging to localize blood vessels, image analysis to reconstruct vessels in 3-D, and miniaturized robotics to place a needle in the center of the indicated vein. The design of the current robot has been previously described in Refs. 25 and 26. These manuscripts also describe the cannulation process in detail and present vessel puncture success rates on tissue phantoms. Following the robotically guided venipuncture, the blood sample is then extracted and transferred to the analysis unit, which provides blood measurements on sample volumes of 25 μl using microcentrifugation and optical detection. Currently, the device is aimed at performing key components of the complete blood count — specifically, a 3-part white blood cell differential and hemoglobin measurement[27].

Table 1 Summary of key sub-systems in the integrated device.

	Venipuncture robot	Sample handling	Blood analyzer unit
Function	Locate and cannulate blood vessel	Extract sample and transfer to analyzer	Obtain measurements of hematology
Features	– NIR/US imaging – Robotic gantry – Needle manipulator	– Peristaltic pump – Tube switching – Sample dispenser	– Plastic acrylic chip – Miniature centrifuge – Fluorescent microscope

These are two of the most commonly requested blood tests in the U.S.[28].

In this paper, we describe key features of the integrated device, present results assessing the blood analyzer and sample handling module through a series of *in vitro* experiments, and finally demonstrate feasibility of the integrated platform using tissue phantoms infused with a blood mimicking fluid (BMF).

3. RESULTS

3.1 Microcentrifugal blood separation and analysis

The analyzer consists of an acrylic chip to house the sample, a centrifuge to fractionate the blood, and an optical microscopy detection system to quantify white cells. A miniaturized centrifuge is used to spin the acrylic chip at 10,000 rpm to separate the cellular components from plasma.

Single-use disposable chips house the blood sample and are fabricated using three layers of cast acrylic sheets which are laser cut and bonded into 104 mm chips, measured lengthwise. The top and bottom layers are 1.5 mm thick, whereas the middle layer is 0.9 mm thick. The chip geometry consists of a 2 mm wide detection channel and a circular reservoir chamber at the distal end of the channel. After centrifugation, the reservoir holds the packed red blood cells, and a band of white cells sits atop this layer in the detection channel. To image the white cell layer, a miniaturized fluorescent microscope was developed[27]. After the white cell layer is detected by the system and brought into focus, an image processing step is performed and the thickness of the white cell region is quantified. The software then compares this measured thickness with pre-determined values to compute white cell counts.

We evaluated the reliability of the blood analyzer using a simulated white cell assay, in which the total area of the buffy coat was correlated with a cell count to generate a standard curve. We used a BMF solution spiked with fluorescently labeled microbeads (ø15 μm) to simulate white cells, and a 9% glycerol solution (density = 1.26 g/cm^3) to simulate a packed red cell fluid (see Section 5.1 for a detailed description of the BMF sample preparation protocol). The bead counts per microliter of sample were 100, 200, and 300.

First, 25 μl of sample was manually pipetted into the acrylic chip and loaded into the analyzer. The centrifuge was then spun at 10,000 rpm for 5 minutes. Following centrifugation, the microscope scanned the detection channel for the fluorescing buffy coat. Once the salient layer of packed beads was found, a series of image processing steps were performed to enhance, segment, and

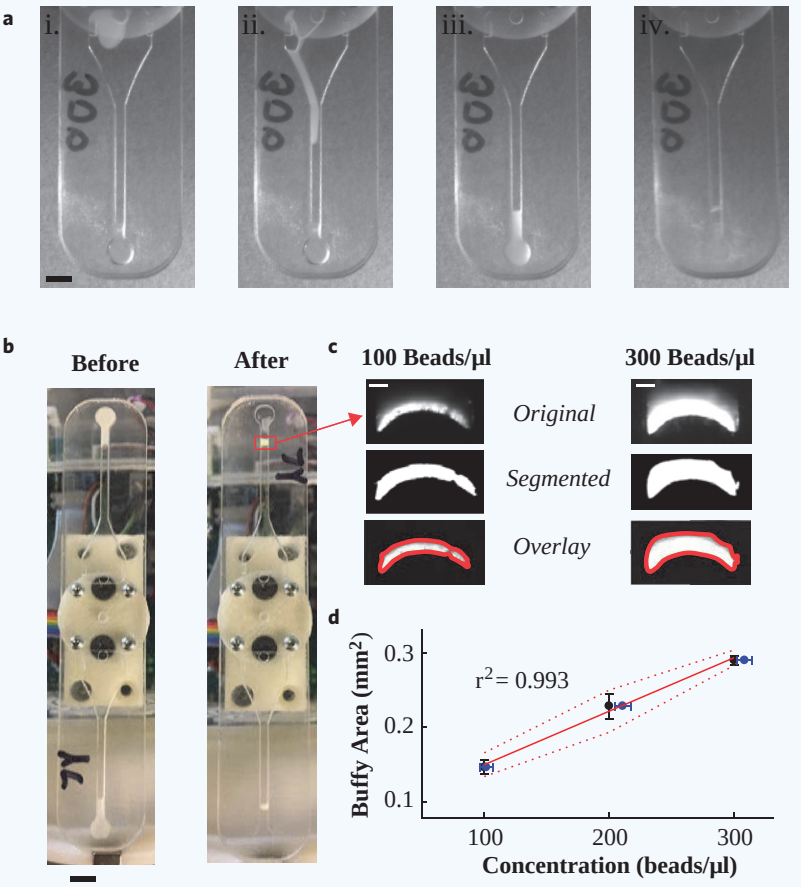

Figure 2 Analysis of a simulated white blood cell assay using density centrifugation, fluorescence microscopy, and image processing. (**a**) Image time series showing the formation of the buffy coat in the detection channel (scale bar = 4 mm). (**b**) Before and after centrifugation of BMF solution (scale bar = 6 mm). (**c**) Original and processed images of the buffy layer (scale bar = 0.4 mm). (**d**) Standard curve for the bead-simulating white cell assay; solid and dotted red lines represent linear fit and 90% Confidence Intervals (CI) respectively (mean of n = 3, error bars represent Standard Deviation (SD)). Accuracy of bead counts was compared against manual measurements via hemocytometer, plotted on the x-axis (blue points, mean of n = 3, error bars represent SD).

measure this region (see Section 5.4.4 for a detailed description of the image processing steps).

Figure 2b shows the three-layer acrylic chip containing the BMF sample before and after centrifugation. The resulting images of the fluorescently labeled beads and the corresponding segmented areas are shown in **Fig. 2c**. The standard curve in **Fig. 2d**, was produced from plotting the measured buffy coat area with known bead concentrations in each sample, resulting in a coefficient of variation of 0.993. Standard deviations in the measured area were 6.43%, 7.32%, and 2.12% of the mean for 100, 200, and 300 beads/μl, respectively.

High consistency between trials suggests that 25 μl of sample was sufficient for our analysis. Furthermore, commercial HemoCue devices use as little as 10 μl of sample for white blood cell analysis, which has been shown to be sufficient[16,29]. The bead concentration was varied from 100–300 beads/μl to challenge the capabilities of our blood analysis approach. Specifically, with a lower number of beads (or cells) in the sample, a thinner buffy coat is formed after centrifugation, and thus it is more difficult to segment and quantify the buffy coat area. In previous work, we demonstrated feasibility of our blood analysis approach using porcine blood samples with clinically relevant cell concentrations[27].

3.2 Sample extraction and delivery to the blood analyzer

The objective of the sample handling module is to transfer the extracted blood sample to the analyzer unit. To accomplish this, we designed a tube switching mechanism and dispenser that uses a peristaltic pump to deliver samples to the diagnostic chip and clean the tubing with a saline wash fluid.

As seen in **Fig. 3**, the pump design consists of a base platform, containing the tube switch mechanism, sharps container, and saline wash fluid bottle. After the venipuncture robot performs the needle insertion, the peristaltic pump activates to transfer the sample to the fluid dispenser for delivery to the analysis chip.

The sample dispenser functions to deliver the blood sample to the analysis chip. The design, as seen in **Fig. 4**, consists of a rotating tube arm, which serves as the main support structure, and a mechanism to lower and raise the dispenser nozzle over the inlet of the analysis chip. **Figure 4a** shows the tube switch pump and sample dispenser integrated with the blood analyzer (see Section 5.6 for a detailed description of the Sample Handling Module).

Experiments were conducted to investigate the loss of fluorescent beads in the BMF solution during the sample handling process. The system was designed to minimize cell loss while transferring the sample from the venipuncture robot to the blood analyzer. For these experiments, we created three sets of BMF samples spiked with known concentrations of fluorescent beads. Each set contained concentrations of 100, 200, and 300 beads/μl (see Section 5.1 for a detailed description of the BMF sample preparation protocol). For each concentration, 1 ml of solution was pumped through the sample handling module and collected at the nozzle of the dispenser unit. Another, 1 ml drawn from the same solution, was used as a control. In both cases, bead counts were obtained using a hemocytometer. Results from the processed and control groups are shown in **Fig. 5** (n = 3 for each bead set). The percent difference in bead counts for the 100, 200, and 300 bead/μl concentrations were 3.88%, 2.90%, and 0.37%, respectively. Using a two-sample t-test, there was no significant difference in bead counts between the processed and control groups (p = 0.47, p = 0.83, p = 0.98 for 100, 200, and 300 beads/μl, respectively).

3.3 Integrated device

The last set of experiments were conducted on the integrated device — from sample draw to analysis — using blood vessel phantoms and BMF spiked with fluorescent particles. Here, we demonstrated the integration of the venipuncture device, sample handling module, and blood analyzer unit. **Figure 6a** shows the experimental setup, **Fig. 6b** depicts key steps in the process, and **Table 2** summarizes the time-to-completion for each step. **Video 1** demonstrates the functionality of the integrated device.

Video 1 can be viewed at http://www.worldscientific.com/doi/suppl/doi:10.1142/S2339547818500048. This video depicts the automated blood draw and analysis device. First, the venipuncture robot is seen loading the disposable needle and US gel clip onto the manipulator. Next, the venipuncture robot rotates over to a vessel phantom perfused with blood mimicking fluid spiked with fluorescent microbeads, and performs the cannulation under image guidance. The sample handling module then extracts, pumps, and delivers the sample to the blood analyzer unit. Once dispensed in the microfluidic chip, the mini-centrifuge is used to fractionate the sample and suspend the microbeads in the middle of the detection channel. Finally, an inverted microscope is positioned under the layer of fluorescing microbeads to measure and quantify the number of beads in the sample.

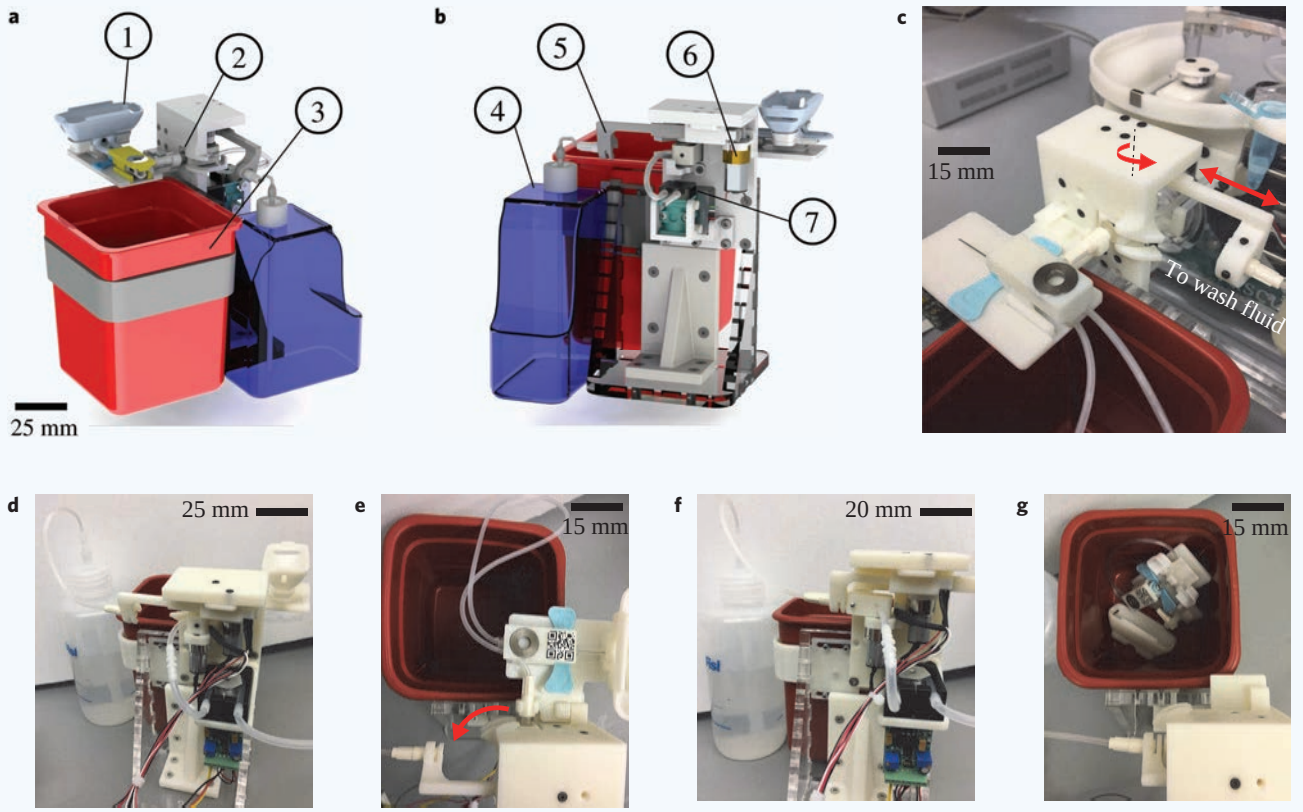

Figure 3 Peristaltic pumping system used to transfer samples from the venepuncture robot to the blood analyzer. (**a**) Front view, highlighting the: consumables cartridge (1), butterfly needle tube connector interface (2), and sharps container (3). (**b**) Back-view, highlighting the: saline wash container (4), wash fluid connector rack (5), DC gearmotor to actuate the rack and pinion mechanism (6), and peristaltic pump mounted to the back of the unit (7). (**c**) Pumping system integrated with the blood analyzer. (**d–g**) Clinical workflow. (**d**) Butterfly needle hub connected to the pump via the tube switching piece. (**e**) Consumables handling for the venipuncture robot. (**f**) Tube switching piece rotates 90°, and the rack translates to attach the wash fluid connector. Wash fluid can then be pumped through the system using the peristaltic pump. (**g**) Consumables disposed in sharps container after procedure.

The device was tasked with cannulating a 3 mm diameter blood vessel phantom (see Section 5.3 for details), collecting the BMF, transferring the sample to the blood analyzer, and quantifying the bead concentration via density centrifugation and fluorescence imaging. Six trials for each bead concentration (100, 150, 200, 250, and 300 beads/μl) were used for the study. As in the previous experiments, 25 μl were dispensed for each trial onto the centrifuge chip and spun at 10,000 RPM for 5 minutes. After spinning, the fluorescent buffy coat was imaged and segmented to measure the area. This area was then used to quantify the bead concentration using the standard curve obtained in earlier experiments. Results are shown in **Fig. 7**. The standard deviation between predicted and pre-determined bead concentrations for 100, 150, 200, 250, and 300 beads/μl samples were 7.00%, 3.20%, 5.40%, 4.49%, and 4.56%, respectively ($n=6$ for each bead set). Additionally, cannulation accuracy was 100% for the 30 trials, where a successful puncture was defined as visualizing sample flashback in the hub of the butterfly needle.

4. DISCUSSION

In this paper, we presented the development of an automated blood draw and analysis device, and evaluated the system through a series of *in vitro* experiments. We developed a standard curve for an absolute white blood cell assay using a BMF solution spiked with fluorescent beads, correlating buffy coat areas with known bead concentrations. Our approach utilized density centrifugation, fluorescense microscopy, and image processing. Next, we demonstrated minimal loss of microbeads through the sample handling module after collection of the BMF solution. This ensured that the number of beads dispensed in the chip was similar to that in the original sample. Lastly, combining the three major components of the system, we showed results from the white blood cell assay using a range of bead concentrations, by referencing the standard curve created in earlier experiments. These tests included sample collection via the venpuncture robot, pumping via the sample handling module, and analysis via the blood analyzer unit. Altogether, the results indicate a robust platform that merges the benefits associated with laboratory automation and point-of-care diagnostics. Furthermore, our relatively simple chip design and analysis method was selected to minimize the chance of failure on human samples, whereas other microfiltration techniques could be more susceptible to clogging and variability in the size of white blood cells.

For diagnostic laboratories, the device is compact and less expensive compared to full, backroom automation systems, and in the future, can be extended to incorporate a broader panel of assays. This would involve redesigning the acrylic chip by modifying the channel geometries, as well as incorporating additional reagents. Further miniaturization of the integrated device, such as designing the pumping system and analyzer into the base of the venipuncture robot, would make the device more applicable to hospital and ambulatory settings. Finally, future validation work includes testing with discarded human blood samples infused through phantom vessels, and evaluating the full device in humans — from blood draw to analysis.

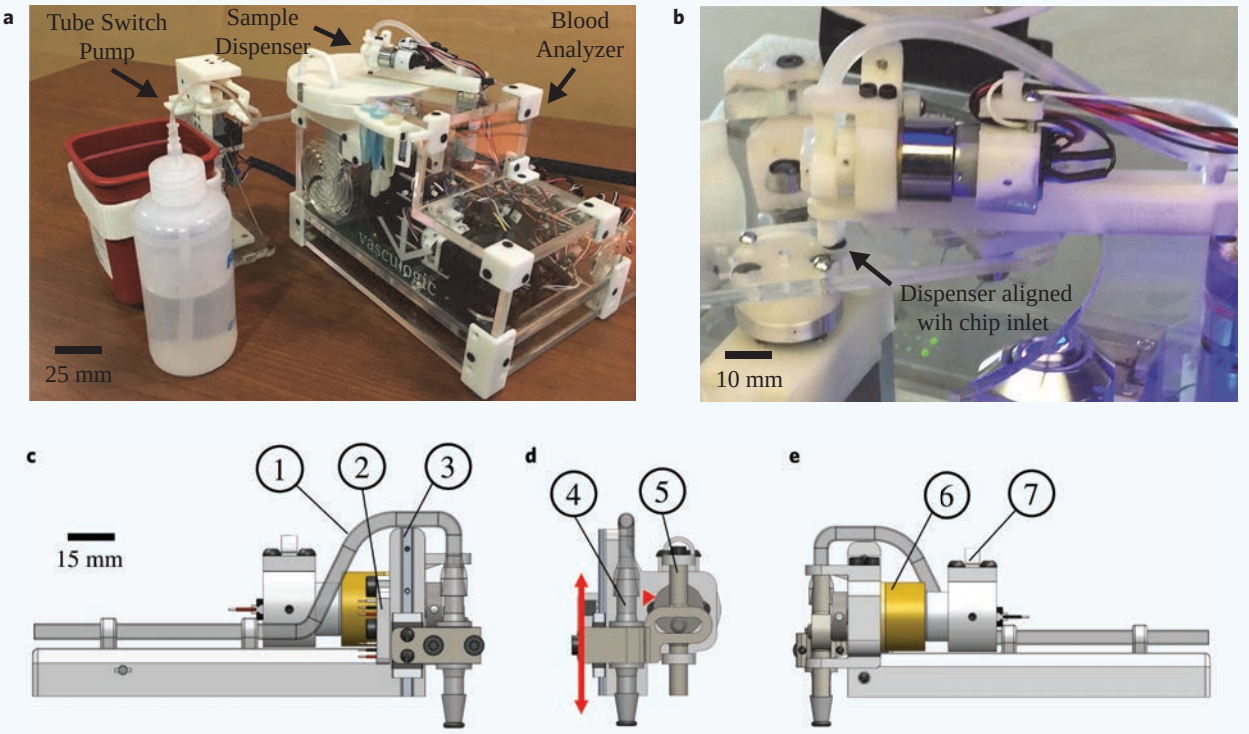

Figure 4 Sample dispenser design. (**a**) Location of the dispenser relative to the tube switch pump and blood analyzer. (**b**) Dispenser delivering sample to the chip. (**c**) Right view, highlighting the: tube leading from the peristaltic pump to the dispenser nozzle (1); Position sensors used to indicate when the dispenser has reached one of two states: raised or lowered (2); and the linear rail and corresponding carriage used to guide the vertical motion (3). (**d**) Front view, highlighting the: plastic nozzle with an O-ring attached to the bottom to achieve a leak-proof seal with the acrylic chip (4); and Scotch-yoke mechanism used to convert rotational motion into linear translation (5). (**e**) Left view, highlighting the: motor used to actuate the mechanism (6); and a strain relief for the sensor and motor wires (7).

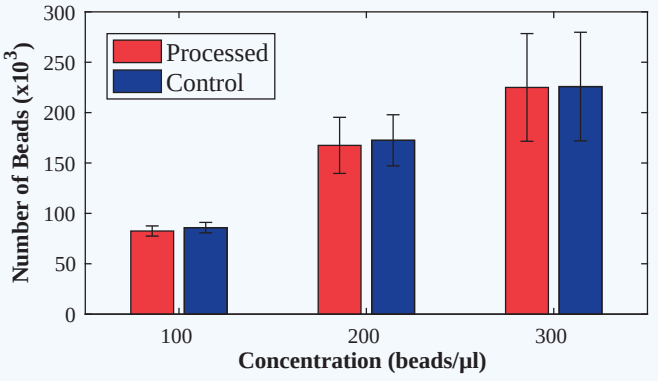

Figure 5 Loss of beads during the sample handling process. For each bead concentration ($n = 3$), no significant differences were found between the processed and control groups using a two-sample t-test ($p = 0.47$, $p = 0.83$, $p = 0.98$ for 100, 200, and 300 beads/μl, respectively).

5. MATERIALS AND METHODS

5.1 Blood mimic sample preparation

The sample to mimic blood was prepared by adding fluorescence bead suspension (polystyrene bead density = 1.06 g/cm^3, F21010, Thermo Fischer) and Glycerol solution (density = 1.26 g/cm^3, 49781, Sigma Life Science) to a BMF solution (model 046, lot # 18GU-039, Tissue Simulation Tech). The concentration of glycerol was 9% v/v and beads were added to prepare final solutions. Fluorescently labeled beads (ø = 14.6 ± 0.15 μm) were used as representation of white blood cells, whereas Glycerol was used to create the density difference between the solution and beads. Each solution was vortexed for 2 minutes prior to mixing and the final solution was vortexed for 3 minutes during preparation and before use to ensure a uniform bead distribution.

5.2 Manual bead count verification

The concentration of beads in the sample before and after use was determined using a hemocytometer (Cat#:1492, Hausser Scientific). A 10 μl of sample solution was injected in the hemocytometer without dilution and imaged using a florescence microscope (IX81, Olympus). The average bead count in four cells of the hemocytometer, identified by overlaying phase and green florescence images, was used to calculate final concentration of beads per microliter.

5.3 Fabrication of tissue phantoms

Blood vessel phantoms were composed of silicon tubing (11-189-15H, Fisher Scientific) with an inner and outer diameter of 1.98 mm and 3.18 mm, respectively. Phantom skin tissue consisted of an 18% gelatin concentration derived from porcine skin (G2500-1KG, Sigma Life Science). The gelatin solution underwent four heating cycles (5 seconds each) in a 1200 W microwave, and was then placed in a 10 × 20 × 1.5 cm 3D-printed

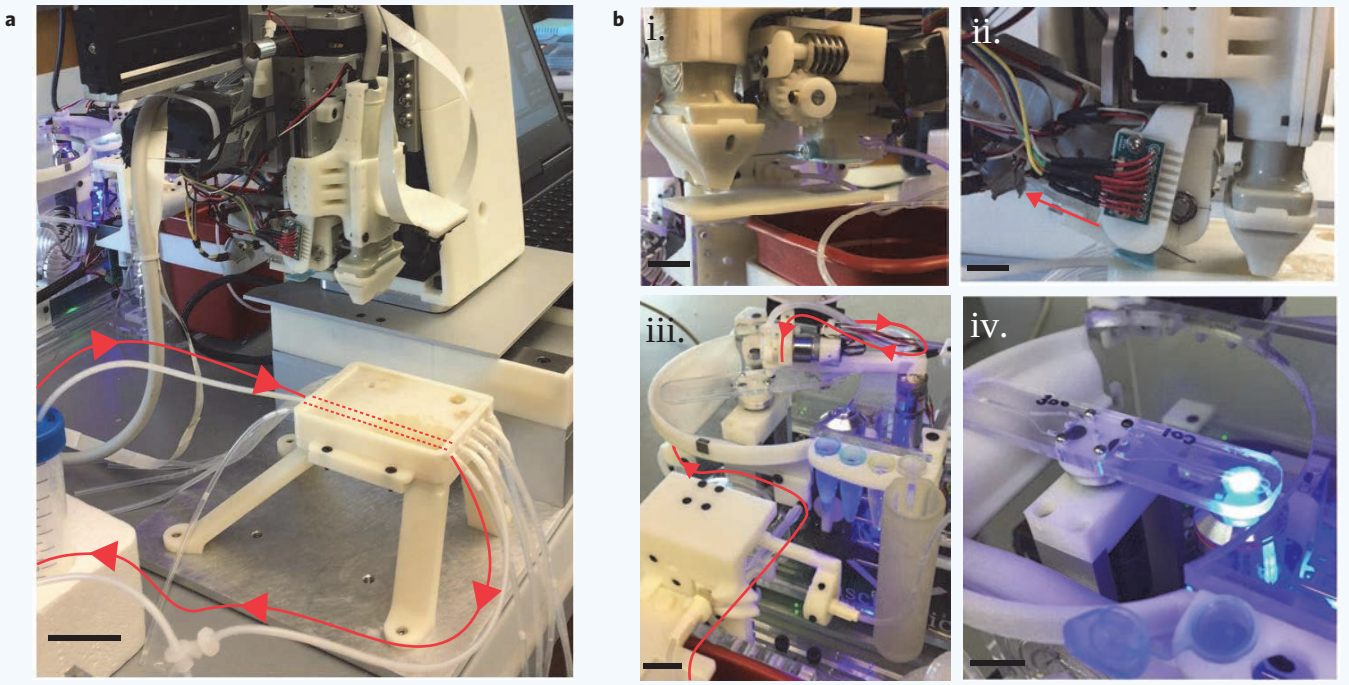

Figure 6 Integrated device testing. (**a**) Experimental setup showing the venipuncture robot and phantom. The BMF solution is pumped through the phantom vessels to simulate venous blood flow. Red arrows indicate flow direction (scale bar = 25 mm). (**b**) Key steps: i. The venipuncture robot picks up the needle clip via an electromagnetic mechanism (scale bar = 10 mm). ii. The robot inserts a needle into the vessel and extracts 3 ml of sample (scale bar = 10 mm). iii. The sample is pumped to the blood analyzer, where a 25 μl sample is dispensed onto the chip (scale bar = 15 mm). iv. The sample is spun and the device aligns the detection channel with the microscope to image and quantify the buffy coat (scale bar = 15 mm).

Table 2 Time-to-completion for each step in the integrated device. Pump switching to the wash nozzle (step 5) and cleaning of the pump tubing (step 6) occur during centrifugation of the chip (step 4).

Step	Description	Time (s)
1	Robotic needle insertion	6
2	Sample collection via pump	10
3	Sample dispensed onto chip	2
4	Centrifugation of chip	300
5	Pump switching to wash nozzle	2
6	Cleaning of pump tubing	35
7	Imaging of buffy coat	5

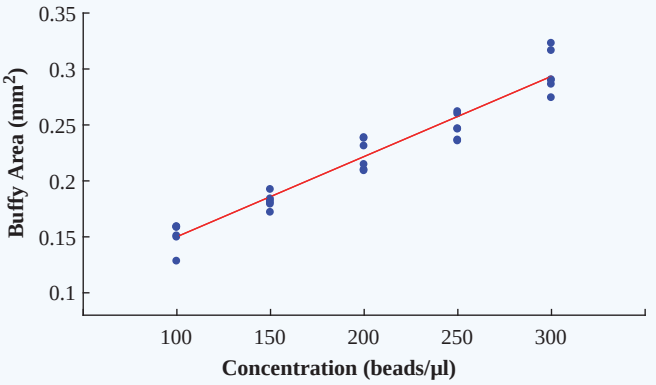

Figure 7 Integrated device testing results. Buffy coat area of BMF samples relative to the standard curve. The solid red line shows the standard curve, and the blue dots indicate the measured buffy coat area ($n = 6$ for each bead set).

box, containing the silicon tubing in order to solidify. The phantom vessels were placed at a depth of 2 mm, measured from the gelatin surface to the outer wall of the tubing. More details associated with the fabrication of tissue phantoms can be found in Chen *et al.*[30]. The BMF solution was pumped through the blood vessel phantoms via a peristaltic pump (12 V, #1150, Adafruit Industries) at a rate of 35 ml/min, approximating the resting venous flow rate of healthy adults.

5.4 Design details of the blood analyzer

5.4.1 *Centrifuge*

The centrifuge was driven by a brushless servo motor (EC-16, Maxon Motors) with an attached encoder to provide position and velocity control. Machined brackets were used to mount the motor to an aluminum base, which also served as the mounting plate for the enclosure of the blood analyzer unit.

5.4.2 *Acrylic chip*

Layers of the acrylic chip were bonded using 100 μm thick pressure-sensitive adhesive (DFM 100, FLEXcon) and pressed together under

5 MPa of pressure at 65 °C using a heat press (Clam shell, PowerPress). Corona discharge (BD-10A, Electro-Technic) was used to surface treat and enhance the wettability of the substrate, allowing the sample to easily flow into the channels.

5.4.3 *Fluorescent microscope*

The fluorescent imaging system was mounted on two linear stages (LSM025 and LSA25, Zaber) to provide translation along the length of the detection channel and in the vertical direction. The excitation optics included a high-powered blue LED (CreeXPEBlu-1, LED Supply), excitation filter (475 ± 35 nm, Semrock), dichroic mirror (506 nm beam splitter, Semrock), and a 4x objective lens (0.10 NA, RMS4x). The emission optics include, an emission filter (529 ± 24 nm, Semrock), a tube lens (f = 50 mm, AC127050A, Thorlabs), and a CMOS monochrome camera (FMVU-03MTM-CS, Point Grey) to capture the reflected light.

5.4.4 *Buffy coat segmentation and quantification*

Segmentation of the fluorescent buffy coat was performed using the following image processing steps: linear contrast stretching, 2-D order statistic filtering, thresholding via Otsu's global method[31], morphological post-processing, and object area quantification. This was all accomplished in the LabVIEW programming environment. The pixel area of the segmented buffy coat was quantified, and converted to metric units using a pre-determined calibration constant. This constant was obtained using a micrometer calibration slide (MR400, AmScope).

5.5 Design details of the venipuncture robot

The robot consisted of a 6-DOF base positioning system: the prismatic joints form a 3-DOF Cartesian gantry, whereas the revolute joints align the end-effector with the vessel orientation. The end-effector included a pair of calibrated stereo cameras (VRmMS-12, VRmagic), an 18 MHz Doppler US transducer (L1830, Telemed), and a 3-DOF motorized needle manipulator that introduces the cannula into the center of the vessel[26]. The system was programmed using LabVIEW control software and runs on a laptop computer (i7-4710HQ 2.5 GHz CPU), where the image processing is accelerated on an embedded GPU (Nvidia Quadro K2200M).

5.5.1 *Needle manipulator*

The 3-DOF needle manipulator is used to guide the cannula into the center of the vessel. A linear stage adjusts the height of the needle, a worm gear mechanism sets the insertion angle, and a linear spindle controls the needle insertion. During the cannulation, insertion forces are monitored normal to the needle tip along a single axis using a force sensor (FSG-5N, Honeywell) with a resolution of 0.01 N. Peaks in the force profile can be observed when the needle punctures the skin, and subsequently the vein, indicating a successful venipuncture.

5.5.2 *Automated consumables handling*

To remove practitioner contact with exposed sharps and contaminated material, an automated consumables handling system was developed. The first consumable, which allows the robot to adapt to a range of needles, is a universal needle clip (**Fig. 8a, left**). The second consumable (**Fig. 8a, right**) is a clip containing sterile, solid agarose gel which serves as the acoustic transmission material for the US probe. Using a solid gel eliminates the need to apply a liquid gel onto the patient's arm.

The configuration of the robot was designed to simultaneously load the needle and US gel clip on the manipulator in a single, automated step. Once the clinician places the consumables package in the indicated holder behind the device, the robot rotates the manipulator over the package (**Fig. 8d**). Then, in one motion, the manipulator attaches the needle via an electromagnet, while securing the US gel clip via a press-fit (**Fig. 8e**). After the procedure, the needle and US gel clip are disposed in a sharps container next to the venipuncture device.

5.6 Design details of the sample handling module

5.6.1 *Tube switch pump*

The work-flow for using this pump with the venipuncture device is as follows. After the disposable cartridge containing the needle and US gel clip is loaded into the device, the back-end of the needle tubing automatically connects to the tube switch mechanism via a press-fit latch.

After the venipuncture, the needle is withdrawn from the vessel and disposed with the US gel clip into a sharps container located next to the sample handling module. At the same time, the motor on the tube switch mechanism rotates the needle tubing over a guide rail to release the tube connector from the press-fit, and into the sharps bin. A second motor then translates the tube connector interfacing with the wash fluid container. Altogether, this allows the sample handling module to dispose the contaminated components, and prepare for the wash step.

Once the rack translates enough so the wash fluid connector is pressed into the tube switching piece, the peristaltic pump activates again; this time, flushing the tubing with saline fluid. Finally, the dispenser on the

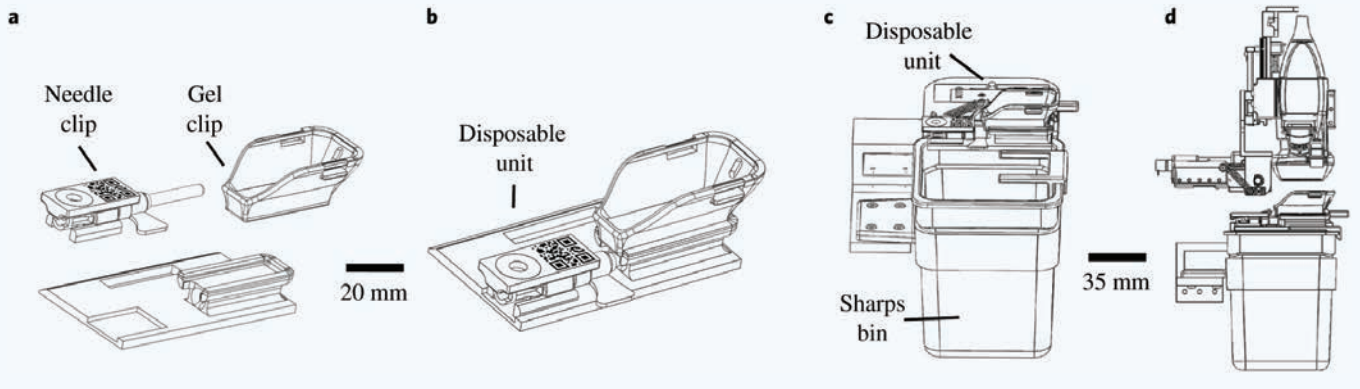

Figure 8 Automated needle handling and consumables system. (**a**) The re-loader unit depicting how the needle and gel clip attach to the tray, and (**b**) the pre-packaged form of the disposable. (**c**) The re-loader system showing the disposable unit integrated with a sharps bin, mounted to the back of the device. (**d**) The manipulator positioned above the re-loader, showing how it would attach the needle and US gel.

back-end of the pump rotates over to a waste fluid container to dispense the fluid.

5.6.2 *Sample dispenser unit*

A Scotch-yoke mechanism was implemented to convert the actuated rotational motion to linear, vertical motion. This mechanism allows the nozzle to translate 5 mm — sufficient for pressing against the blood analysis chip and for clearing the top surface of the diagnostic device as the dispenser rotates to the chip inlet and waste container. Specifically, the dispenser rotates 60° from the home position — by the waste container — to deliver the blood sample to the analysis chip. This motion is achieved by an actuator embedded in the diagnostic device, in which the dispenser is attached.

Two magnetic-based Hall-effect sensors are installed behind the linear carriage, and a small magnet is embedded in the dispenser clamp. Together, this forms the hardware of the position control scheme used to lower and raise the dispenser nozzle. Two, discrete system states are programmed into the control software: nozzle raised and lowered. The gearmotor is commanded to activate until the sensor is triggered, indicating the nozzle has reached the desired position.

ACKNOWLEDGMENTS

This research was supported by the U.S. National Institutes of Health (R01-EB020036). The work of M. Balter was supported by an NSF Graduate Research Fellowship (DGE-0937373) and the GAANN Training Program in Emerging Areas of Precision and Personalized Medicine (P200A150131). The work of J. Leipheimer was supported by the NIH/NIGMS Rutgers Biotechnology Training Program (T32 GM008339). The work of A. Chen was supported by the NIH/NIGMS Rutgers Biotechnology Training Program (T32 GM008339), and an NIH F31 Predoctoral Fellowship (EB018191).

REFERENCES

1. Kidd, B.A., Hoffman, G., Zimmerman, N., Li, L., Morgan, J.W., Glowe, P.K., Botwin, G.J., Parekh, S., Babic, N., Doust, M.W., Stock, G.B., Schadt, E.E. & Dudley, J.T. Evaluation of direct-to-consumer low-volume lab tests in healthy adults. *J. Clin. Invest.* **1**(8), 1–11 (2016).
2. The Freedonia Group, *In Vitro Diagnostics in the U.S.*, Vol. 59 (2011).
3. Niska, R., Bhuiya, F. & Xu, J. National hospital ambulatory medical care survey: 2007 emergency department summary. National Health Statistics Report, pp. 1–31 (2010).
4. Hammerling, J. A review of medical errors in laboratory diagnostics and where we are today. *Lab. Med.* **43**(2), 41–44 (2012).
5. Pati, H.P. & Singh, G. Turnaround time (tat): Difference in concept for laboratory and clinician. *Indian J. Hematol. Blood Transfus.* **30**(2), 81–84 (2012).
6. Stotler, B.A. & Kratz, A. Determination of turnaround time in the clinical laboratory: "Accessioning-to-result" time does not always accurately reflect laboratory performance. *Am. J. Clin. Pathol.* **138**(5), 724–729 (2012).
7. Zhi, M., Ding, E.L., Theisen-Toupal, J., Whelan, J. & Arnaout, R. The landscape of inappropriate laboratory testing: A 15-year meta-analysis. *PLoS One* **8**(11), 1–8 (2013).
8. Lippi, G. & Cadamuro, J. Novel opportunities for improving the quality of preanalytic phase. A glimpse to the future? *J. Med. Biochem.* **36**, 1–6 (2017).
9. Kuensting, L.L., DeBoer, S., Holleran, R., Shultz, B.L., Steinmann, R.A. & Venella, J. Difficult venous access in children: Taking control. *J. Emerg. Nurs.* **35**(5), 419–424 (2009).
10. Schwartz, D. & Raghunathan, K. Difficult venous access. *Pediatr. Anesthesiol.* **19**(1), 60 (2009).
11. Frey, A.M. Success rates for peripheral i.v. insertion in a children's hospital. Financial implications. *J. Intraven. Nurs.* **21**(3), 160–165 (1998).
12. Chin, C., Linder, V. & Sia, S. Commercialization of microfluidic point-of-care diagnostic devices. *Lab Chip* **12**(12), 2118–2134 (June 2012).
13. Jung, Y.-J., Gonzalez, J. & Godavarty, A. Functional near-infrared imaging reconstruction based on spatiotemporal features: Venous occlusion studies. *Appl. Optics* **54**(13), 82–90 (2015).
14. Martin, C.L. i-STAT — Combining chemistry and haematology in PoCT. *Clin. Biochem. Rev.* **31**(3), 81–84 (2010).
15. Rao, L.V., Ekberg, B.A., Connor, D., Jakubiak, F., Vallaro, G.M. & Snyder, M. Evaluation of a new point of care automated complete blood count (CBC) analyzer in various clinical settings. *Clin. Chim. Acta* **389**(1–2), 120–125 (2008).
16. Osei-Bimpong, A., Jury, C., McLean, R. & Lewis, S.M. Point-of-care method for total white cell count: An evaluation of the *HemoCue WBC* device. *Int. J. Lab. Hematol.* **31**(6), 657–664 (2009).
17. Cable, R.G., Steele, W.R., Melmed, R.S., Johnson, B., Mast, A.E., Carey, P.M., Kiss, J.E., Kleinman, S.H. & Wright, D.J. The difference between fingerstick and venous hemoglobin and hematocrit varies by sex and iron stores. *Transfusion* **52**(5), 358–366 (2012).
18. Plebani, M. Evaluating and using innovative technologies: A lesson from Theranos? *Clin. Chem. Lab. Med.* **53**(7), 961–962 (2015).
19. Bond, M. & Richards-Kortum, R. Drop-to-drop variation in the cellular components of fingerprick blood: Implications for point-of-care diagnostic development. *Am. J. Clin. Pathol.* **144**(6), 885–894 (2015).
20. Loewenstein, D., Stake, C. & Cichon, M. Assessment of using fingerstick blood sample with i-STAT point-of-care device for cardiac troponin I assay. *Am. J. Emerg. Med.* **31**(8), 1236–1239 (2013).
21. Kricka, L.J., Polsky, T.G., Park, J.Y. & Fortina, P. The future of laboratory medicine — A 2014 perspective. *Clin. Chim. Acta* **438**, 284–303 (2015).
22. Melanson, S.E.F., Lindeman, N.I. & Jarolim, P. Selecting automation for the clinical chemistry laboratory. *Arch. Pathol. Lab. Med.* **131**(7), 1063–1069 (2007).
23. Hawker, C. Laboratory automation: Total and subtotal. *Clin. Lab. Med.* **27**(4), 749–770 (2007).
24. Holland, L.L., Smith, L.L. & Blick, K.E. Total laboratory automation can help eliminate the laboratory as a factor in emergency department length of stay. *Am. J. Clin. Pathol.* **125**(5), 765–770 (2006).
25. Chen, A., Balter, M., Maguire, T. & Yarmush, M. Real-time needle steering in response to rolling vein deformation by a 9-DOF image-guided venipuncture robot. In *IEEE/RSJ International Conference on Intelligent Robots and Systems*, pp. 2633–2638 (2015).
26. Balter, M.L., Chen, A.I., Maguire, T.J. & Yarmush, M.L. Adaptive kinematic control of a robotic venipuncture device based on stereo vision, ultrasound, and force guidance. *IEEE Trans. Ind. Electron.* **64**(2), 1626–1635 (2017).
27. Balter, M.L., Chen, A.I., Colinco, C.A., Gorshkov, A., Bixon, B., Martin, V., Fromholtz, A., Maguire, T.J. & Yarmush, M.L. Differential leukocyte counting via fluorescent detection and image processing on a centrifugal microfluidic platform. *Anal. Methods* **8**(47), 8272–8279 (2016).
28. Osei-Bimpong, A., McLean, R., Bhonda, E. & Lewis, S. The use of the white cell count and haemoglobin in combination as an effective screen to predict the normality of the full blood count. *Int. J. Lab. Hematol.* **34**(1), 91–97 (2012).
29. Russcher, H., van Deursen, N. & de Jonge, R. Evaluation of the HemoCue WBC diff system for point-of-care counting of total and differential white cells in pediatric samples. *Ned. Tijdschr. Klin. Chem. Labgeneesk.* **38**(3), 140–141 (2013).
30. Chen, A., Balter, M., Chen, M., Gross, D., Alam, S., Maguire, T. & Yarmush, M. Multilayered tissue mimicking skin and vessel phantoms with tunable mechanical, optical, and acoustic properties. *Med. Phys.* **43**(6), 3117–3131, 2016.
31. Otsu, N. A threshold selection method from gray-level histograms. *IEEE Trans. Syst. Man. Cybern. Syst.* **20**(1), 62–66 (1979).